This is the accepted manuscript made available via CHORUS. The article has been published as:

Weyl Semimetal Path to Valley Filtering in Graphene

Ahmed M. Khalifa, Ribhu K. Kaul, Efrat Shimshoni, H. A. Fertig, and Ganpathy Murthy

Phys. Rev. Lett. **127**, 126801 — Published 16 September 2021

DOI: 10.1103/PhysRevLett.127.126801

Weyl Semimetal Path to Valley Filtering in Graphene

Ahmed M. Khalifa,[1] Ribhu K. Kaul,[1] Efrat Shimshoni,[2] H.A. Fertig,[3] and Ganpathy Murthy[1]

[1] *Department of Physics and Astronomy, University of Kentucky, Lexington, KY 40506-0055*
[2] *Department of Physics, Bar-Ilan University, Ramat-Gan 52900, Israel*
[3] *Department of Physics, Indiana University, Bloomington, IN 47405*

We propose a device in which a sheet of graphene is coupled to a Weyl semimetal, allowing for the physical access to the study of tunneling from two-dimensional to three dimensional massless Dirac fermions. Due to the reconstructed band structure, we find that this device acts as a robust valley filter for electrons in the graphene sheet. We show that, by appropriate alignment, the Weyl semimetal draws away current in one of the two graphene valleys while allowing current in the other to pass unimpeded. In contrast to other proposed valley filters, the mechanism of our proposed device occurs in the bulk of the graphene sheet, obviating the need for carefully shaped edges or dimensions.

Weyl semimetals (WSMs) [1–5] are three-dimensional materials with an even number of isolated band touching points in the Brillouin zone (BZ) called Weyl nodes. The band dispersion near each Weyl node is that of a massless Weyl fermion, which is chiral, the chirality being encoded in the Berry flux pierced by a surface in momentum space enclosing the Weyl node. Either inversion [1] or time-reveral symmetry [2–5] or both must be broken in WSMs. Many examples of WSM materials are now known [6–8, 10–14].

In monolayer graphene [15] electrons near charge neutrality belong to one of the two Dirac points ($\mathbf{K}$ and $\mathbf{K}'$, related to each other by inversion and time-reversal) which constitute valleys. Due to the large difference in lattice momentum, the valley degree of freedom is highly conserved in transport. This has made it a promising material for use in valleytronics, which seeks to use the valley degree of freedom to encode and manipulate information [16]. Either electrons or excitons can be used to encode information; in the following we will focus on electrons. A necessary first step in this valleytronics program in graphene is to be able to produce valley-polarized current, usually done by valley-filtering an incident valley-unpolarized current. There are many theoretical proposals for doing so. Methods preserving the time-reversal of graphene while breaking inversion [17] include a constriction with tailored edges [18], using the "high-energy" dispersion of electrons away from the Dirac points [19], using strain, which creates an internal gauge field acting oppositely on the two valleys to spatially separate valley currents [20], lattice defects [21] and spin-orbit coupling [22]. Methods that break time-reversal include the use of magnetic and potential barriers [23], or tunnel-coupling monolayer and bilayer graphene with an in-plane magnetic field to tune momentum [24]. Yet other proposals include using adiabatic pumping [25] or Floquet methods [26, 27] to separate the valleys. Most of the proposals need precise control of edges/strain/substrates/superlattices, and/or depend very sensitively on the energy of the electrons to be valley-filtered.

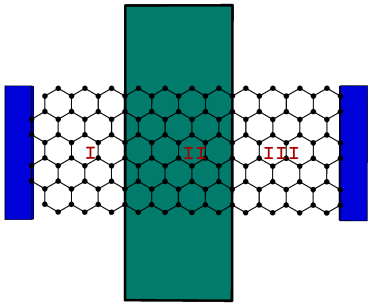

FIG. 1: A schematic picture for a graphene/WSM device. The incoming current (region I) is equally populated in the two valleys and the outgoing current (region III) is valley polarized.

In this Letter we show that the surface of a WSM with three-fold symmetry, breaking both time-reversal and inversion, is a natural substrate for robust valley-filtering current in graphene (see Fig. 1 for the proposed device). The minimal number of Weyl nodes is six. When the chemical potential is at the energy of the Weyl nodes, their projections on the surface BZ (also three-fold symmetric) are points connected by zero energy surface Fermi arc (FA) states (see Fig. 2(a)). Upon doping, the projection of the bulk states at fixed energy on to the surface BZ will be solid regions enclosing the Weyl point projections (WPPs), as shown in Figs. 2(b), 2(c). We refer to these solid regions as "Fermi pockets." We emphasize that: (i) The Fermi pockets break inversion symmetry. (ii) Each $\vec{k}$ in the surface BZ has a continuum of bulk states of the WSM projected on to it. The next step is to weakly tunnel-couple the graphene to the surface of the WSM in their region of overlap, taking care to align it so that the $\mathbf{K}$ Dirac point lies within a Fermi pocket in the surface BZ of the WSM, up to a reciprocal lattice vector of the surface BZ of the WSM, as shown in Fig. 2(d). We emphasize that the $\mathbf{K}'$ point does not overlap a Fermi pocket.

Consider a current injected into the graphene sheet

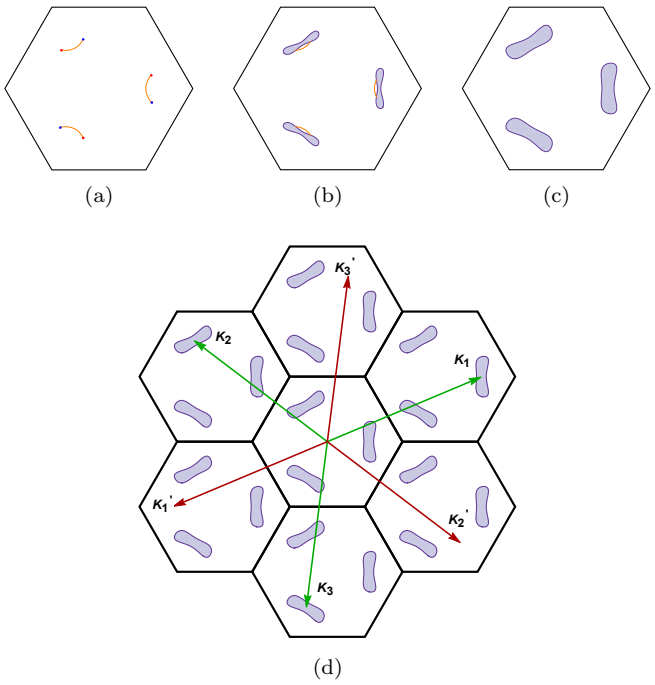

FIG. 2: Evolution of the projected WSM states in the SBZ. (a) At the nodal energy ($E_F = 0$), only the Fermi arcs are present in the SBZ. (b),(c) As the chemical potential is raised, the Fermi arcs get absorbed into the bulk states and eventually disappear in (c). (d) An incommensurate structure of graphene and the WSM shown in momentum space. The green vectors show the three equivalent graphene **K** points. For a range of twist angles, the low-energy states in the **K** valley of graphene lie in a band of the projected bulk states of the WSM. The graphene states near the **K′** points (red vectors) do not overlap the projected bulk states of the WSM in energy, but instead lie in a band gap.

from the left, in region I of the device depicted in Fig. 1. Before it enters region II, where graphene and the WSM are tunnel-coupled, the current is divided equally between the two valleys . When it enters region II, each electronic state in the **K** valley is coupled to (and lies in the middle of) a band of bulk states in the WSM. We assume, plausibly, that the Fermi velocity of graphene is much higher than that of the WSM, implying that all states near the chemical potential μ of the graphene will lie in the middle of the bulk band of the WSM. Each state in the graphene **K** valley will therefore hybridize with them and broaden, resulting in a decay of the current in the **K** valley into the bulk of the WSM, which is assumed to be grounded. By contrast, although the **K′** valley band structure is modified by tunnel-coupling to the WSM, there are no bulk or surface states of the WSM at the same energy, so that the current in this valley will suffer at most a finite diminution due to reflections at the various interfaces of the structure. Note that the greater the length of the tunnel-coupled region, the greater the degree of valley polarization of the outgoing current.

A few remarks are in order about the generality and robustness of our proposal. (i) Without additional symmetries, there is no reason for the chemical potential in the WSM to lie at the Weyl point energy. Thus, generically, the WSM will have Fermi pockets at the surface, as has been experimentally observed [6, 7, 13]. (ii) This implies that the alignment of graphene on the WSM surface can be varied over a range of angles while maintaining the condition that **K** sits within a Fermi pocket, while **K′** does not (see [32] for details). Thus, fine-tuning the alignment of graphene on the WSM surface is not necessary. (iii) Scanning the chemical potential can be achieved by doping the WSM and/or gating graphene. Our proposal will work over a wide range of electron energies near charge neutrality in graphene. (iv) The details of the tunneling matrix elements between graphene and the surface of the WSM are irrelevant: what matters is that each $\vec{k}$ state within the **K** valley is coupled to the WSM continuum. (v) Smooth disorder in the WSM or graphene will scatter single-particle states close in momenta. Since **K** and **K′** are far apart, the valley-filtering will be robust against smooth disorder. (vi) The valley polarization can be detected by using the valley Hall effect [28], by, for example, applying a strain that generates a field acting in opposite directions in the two valleys [20].

Having established the generality and wide applicability of our proposal, in the remainder of this Letter we analyze a specific model of such a device, illustrating the physical behaviors described above. In order to treat arbitrary tunnel coupling strengths via tight-binding, we construct a simple model of the three-fold symmetric WSM, and assume that its surface is commensurate with that of graphene. We treat only the simplest and most symmetric case in the main text, leaving the general case to the supplemental material [32]. We emphasize that our proposal for valley-filtering does not depend on the commensuration we assume for our concrete model.

WSM model.– Our starting point is a minimal two-band model for a Weyl semimetal on a triangular lattice which breaks both time reversal and inversion symmetry, but possesses three-fold rotational symmetry. In momentum space, the Hamiltonian is given by

$$H(\vec{k}, k_z) = \sum_{\mu=x,y,z} f_\mu \sigma_\mu, \tag{1}$$

where $f_x = 2t\left[1 - cos(k_z) + \mu_1 - \sum_{i=1}^{3} cos(\vec{k}.\vec{a_i})\right]$, $f_y = 2t\left[\sum_{i=1}^{3} sin(\vec{k}.\vec{a_i}) - \mu_2\right]$ and $f_z = 2t' sin(k_z)$. Note that $\vec{k}$ here is a two dimensional vector and σ_μ are the usual Pauli spin matrices, and t and t' represent the in-plane and out-of-plane hoppings, respectively. The three $\vec{a}_i$

vectors are the nearest-neigbor vectors on the triangular lattice, $\vec{a}_1 = a\hat{x}$ and $\vec{a}_{2,3} = a(\frac{-1}{2}\hat{x} \pm \frac{\sqrt{3}}{2}\hat{y})$. The 3-fold rotational symmetry of H is manifested in its energy spectrum. The band structure possesses three pairs of Weyl nodes related to one another by 3-fold rotations. These are found at $k_z = 0$, with $\vec{k}$ satisfying $\mu_1 - \sum_{i=1}^{3} cos(\vec{k}.\vec{a_i}) = 0$ and $\sum_{i=1}^{3} sin(\vec{k}.\vec{a_i}) - \mu_2 = 0$. The positions of the Weyl nodes can be moved by varying μ_1 and μ_2. We assume that the free surface of the WSM is in the xy plane, which has three-fold symmetry. The Weyl point projections (WPPs) on to the surface Brillouin zone (SBZ) are connected by Fermi arcs. By standard methods [29] we find the energy dispersion for the Fermi arc states to be

$$E = 2\left[\sum_{i=1}^{3} sin(\vec{k}.\vec{a_i}) - \mu_2\right] \tag{2}$$

Graphene commensurate with the surface of the WSM.– We adopt a model in which the graphene lattice is commensurate with that of the surface of the WSM, and that the WSM lattice constant is smaller than that of graphene. While these assumptions are unrealistic for real materials, they allow us to use the full power of translation invariance to do nonperturbative calculations in the tunnel-couplings without fundamentally changing the character of the system. Calculations for incommensurate lattices are necessarily either perturbative in the tunnel-couplings, or dependent on truncations in momentum space [30, 31], both of which we wish to avoid.

A schematic picture of our commensurate model is shown in Fig. 3. In order to study the electronic properties of this system, we take a finite slab of the WSM in Eq. (1) along the z axis and assume the system to be translationally invariant in the xy plane. Going to real space in the z direction in Eq. (1), we obtain the WSM slab Hamiltonian

$$H_{WSM} = \sum_{n=0}^{N}\sum_{\vec{k}}[C_n^\dagger(\vec{k})M(\vec{k})C_n(\vec{k}) - C_{n+1}^\dagger(\vec{k})TC_n(\vec{k}) - C_n^\dagger(\vec{k})T^\dagger C_{n+1}(\vec{k})], \tag{3}$$

where $C_n(\vec{k})$ is a two-component annihilation operator indexed by layer n and

$$M(\vec{k}) = 2[(1 + \mu_1 - \sum_i \cos\left(\vec{k}.\vec{a_i}\right))\sigma_x + (\sum_i \sin\left(\vec{k}.\vec{a_i}\right) - \mu_2)\sigma_z].$$

Spin has been suppressed for notational convenience. Note that $T = \sigma_x + it'\sigma_y$, N is the thickness of the slab, and that we have set the hopping in the plane our energy unit, $t = 1$. The total Hamiltonian is

$$H = H_{WSM} + H_G + H_t, \tag{4}$$

where H_G is the nearest neighbor hopping Hamiltonian of graphene. H_t allows electrons in graphene to tunnel to the top layer of the WSM in a translation-invariant way.

$$H_t = \sum_{\vec{R}}\sum_{\vec{r}}\left[C_0^\dagger(\vec{r})V_\alpha(|\vec{r} - \vec{R}|)f_\alpha(\vec{R}) + h.c\right], \tag{5}$$

where $C_0(\vec{r})$ is the two-component annihilation operator on the top $n = 0$ layer of the WSM at site $\vec{r}$, and $f_\alpha(\vec{R})$ is an annihilation operator on the sublattice $\alpha = A, B$ at site $\vec{R}$ in graphene.

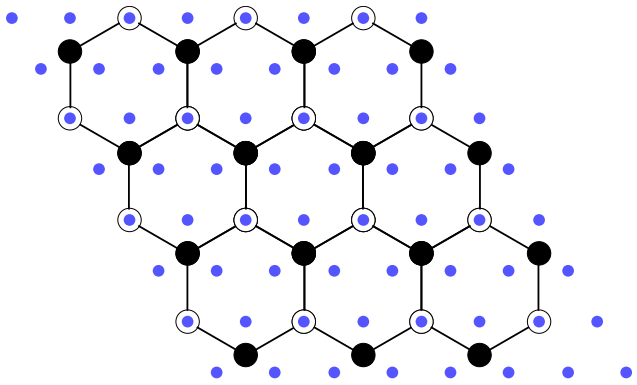

FIG. 3: Graphene and the top surface of our WSM model in a commensurate alignment which we use in our numerical tight binding calculation. Electrons on the A sublattice of graphene (empty circles) are allowed to hop only to the WSM surface site they overlie, while electrons on the B sublattice (solid black) of graphene can hop to the three WSM surface sites surrounding the given B site.

To ensure our requirement that the neighborhood of the **K** point of graphene lies within a bulk band of energies of the WSM we assume that the **K** point of graphene lies on a Fermi arc. From Eq. (2), this is achieved when $\mu_2 = -\sqrt{3}/2$. The **K**′ point will then reside in the gap of the WSM. We then diagonalize Eq. (4) for this value of μ_2 to get the band structure of the system. We restrict ourselves to nearest-neighbor hopping only in H_t. This operationally means that electrons on the A sublattice of graphene hop only to the WSM surface site at the same xy coordinates with a spin-independent amplitude κ, while electrons on the B sublattice of graphene can hop to the three sites of the WSM surface surrounding it with spin-independent amplitude κ'. As we show in the supplemental material [32], moving the Fermi arcs or making the hopping more generic does not make any qualitative difference to our results.

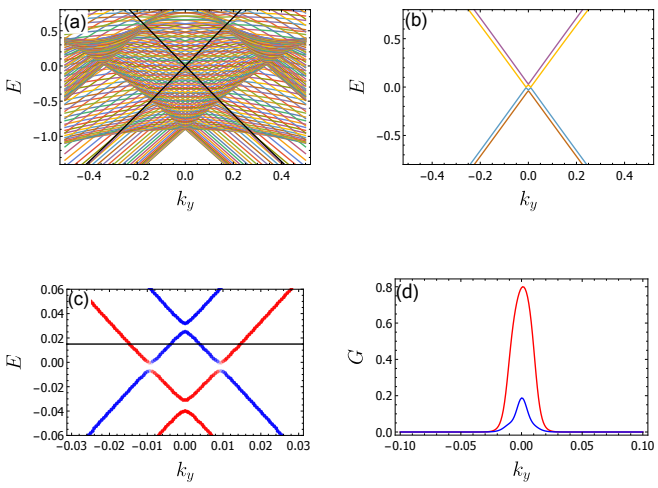

FIG. 4: Results of the tight binding calculation. (a),(b) The graphene/WSM spectrum is shown near the **K** and the **K′** valleys, respectively. The Dirac cone in the **K** valley (shown in black) is immersed in the bulk states of the WSM while the Dirac cone near the **K′** valley is slightly perturbed. (c) An expanded view zooming in on the **K′** valley shows an inverted band structure where the colors code the average of S_z operator with red being spin up and blue spin down. (d) The conductance of the graphene/WSM device based on a simplified model for the states near the **K′** valley is shown in units of e^2/h. The conductance shows partial spin polarization as red denotes spin up states where blue denotes spin down states.

Our tight-binding calculations presented in Fig. 4(a),(b) are consistent with expectations from the generic incommensurate case discussed earlier. We see that the Dirac cone for the **K** valley is immersed in the continuum of the bulk states while the **K′** valley is isolated in the gap. A close examination of Fig. 4(b) reveals induced spin-orbit (SO) coupling, time-reversal breaking, and sublattice symmetry breaking in the states of graphene's **K′** valley.

The tight-binding results show that, at the **K′** valley, the bands split into (almost purely) ↑ and ↓ bands with a band inversion near the **K′** point (Fig. 4(c)). This can lead to interesting consequences for transport: the different sizes of the Fermi surfaces for the two spin species (at the Fermi level marked black in Fig. 4(c)) will lead to different transmission probabilities, and consequently a (partial) spin polarization of the fully valley polarized current.

An effective Hamiltonian for the **K′** valley can be obtained by integrating out the bulk states of the WSM (see the supplemental material for details [32]). The resulting effective Hamiltonian is then used to obtain the Landauer conductance ($G = \frac{e^2}{h}T$, where T is the transmission probability [32]) of the device, shown in Fig. 4 for the two spin channels. We have assumed that there is translation invariance in the y-direction, perpendicular to the current flow. Given our assumptions, the conductance is due to the **K′** valley only. The coupling to the WSM, breaking both sublattice and time-reversal symmetries, results in unequal conductances in the two spin channels.

Conclusions.–We have shown that overlaying graphene on a 3-fold symmetric surface of a WSM breaking both time-reversal and inversion, with an alignment which places the **K** point of graphene in a Fermi pocket of the surface BZ of the WSM while the **K′** point lies outside the Fermi pockets in the first few zones of the WSM in an extended zone scheme (see [32] for details), will lead to a robust valley filter for graphene.

The physics leading to this may be stated concisely: states near the **K** valley of graphene lie within a band of bulk states of the WSM, projected to the surface BZ, hybridizing with the bulk states and "dissolving" into them. Current-carrying electrons in the **K** valley will scatter into bulk states of the (grounded) WSM, carrying them away from the graphene layer. States near the **K′** valley, on the other hand, lie in a bandgap of the WSM, and will remain localized in the graphene, though their transport will be modified by the sublattice and time-reversal breaking induced by the WSM. Thus, for a sufficiently long interface (along the current direction), only the current in the **K′** valley survives. This current is expected to have a nonzero spin polarization, whose precise value depends on the details of the interface coupling. The valley polarization can be detected using the valley Hall effect [28] and strain [20].

Our proposal does not require precise alignment between graphene and the surface of the WSM, precise control of the tunneling at the interface or the chemical potential of the current-carrying electrons. Smooth disorder will not degrade the valley-filtering. Upon doping the WSM appropriately, our proposal will work for Bernal-stacked/twisted bilayer graphene [15] and transition-metal-dichalcogenides [37] as well.

Diverse applications in addition to valley-filtering can also be considered. With small changes, the WSM could be used as a contact that is electrically connected only to one valley, which could be used to probe equilibrium correlated states in the quantum Hall regime of graphene. It would also be interesting to ask how the correlated states in magic-angle twisted bilayer graphene [38] respond when the states near one valley dissolve into the WSM bulk. We hope to address these and other questions in the near future.

We acknowledge support from the National Science Foundation via grant nos. DMR-2026947 (A.M.K and R.K.K.), ECCS-1936406 and DMR-1914451 (H.A.F.), as well as the support of the Research Corporation for

Science Advancement through a Cottrell SEED Award (H.A.F); the US-Israel Binational Science Foundation through awards No. 2016130 (H.A.F, G.M. and E.S.) and 2018726 (H.A.F and E.S.); and the Israel Science Foundation (ISF) Grant No. 993/19 (E.S.).

[1] S. Murakami, New J. Phys. **9**, 356 (2007).
[2] X. Wan, A. M. Turner, A. Vishwanath and S. Y. Savrasov, Phys. Rev. B **83**, 205101 (2011); P. Hosur, S. A. Parameswaran and A. Vishwanath, Phys. Rev. Lett. **108**, 046602 (2012).
[3] K. Y. Yang, Y. M. Lu and Y. Ran, Phys. Rev. B **84**, 075129 (2011).
[4] A. A. Burkov and L. Balents, Phys. Rev. Lett. **107**, 127205 (2011).
[5] G. Xu, H. Weng, Z. Wang, X. Dai, and Z. Fang, Phys. Rev. Lett. **107**, 186806 (2011).
[6] B. Q. Lv, H. M. weng, B. B. Fu, X. P. Wang, H. Miao, J. Ma, P. Richard, X. C. Huang, L. X. Zhao, G. F. Chen *et al*, Phys. Rev. X **5**, 031013 (2015).
[7] S.-Y. Xu, I. Beloploski, N. Alidoust, M. Neupane, G. Bian, C. Zhang, R. Sankar, G. Chang, Z, Yuan, C.-C. Lee *et al*, Science **349**, 613 (2015).
[8] S.-Y. Xu, N. Alidoust, I. Blopolski, Z. Yuan, G. Bian, T.-R. Chang, H. Zheng, V. N. Strocov, D. S. Sanchez, G. Chang *et al*, Nat. Phys. **11**, 748 (2015).
[9] Q. Xu, E. Liu, W. Shi, L. Muechler, J. Gayles, C. Felser, and Y. Sun, Phys. Rev. B**97**, 235416 (2018).
[10] H. Inoue, A. Gyenis, Z. Wang, J. Li, S. W. Oh, S. Jiang, N. Ni, B. A. Bernevig, and A. Yazdani, Science **351**, 1184 (2016).
[11] E. H. Silva Neto, Science **365**, 1248 (2019).
[12] I. Belopolski, K. Manna, D. S. Sanchez, G. Chang, B. Ernst, J. Yin, S. S. Zhang, T. Cochran, N. Shumiya, H. Zheng *et al*, Science **365**, 1278 (2019).
[13] D. F. Liu, A. J. Liang, E. K. Liu, Q. N. Xu, Y. W. Li, C. Chen, D. Pei, W. J. Shi, S. K. Mo, P. Dudin *et al*, Science **365**, 1282 (2019).
[14] N. Morali, R. Batabyal, P. K. Nag, E. Liu, Q. Xu, Y. Sun, B. Yan, C. Felser, N. Avraham, and H. Beidenkopf, Science **365**, 1286 (2019).
[15] A. H. Castro Neto, F. Guinea, N. M. R. Peres, K. S. Novoselov, and A. K. Geim, Rev. Mod. Phys. **81**, 109 (2009).
[16] J. R. Schaibley, H. Yu, G. Clark, P. Rivera, J. S. Ross, K. L. Seyler, W. Yao, and X. Xu, Nature Reviews Materials **1**, 16055 (2016).
[17] D. Xiao, W. Yao, and Q. Niu, Phys. Rev. Lett. **99, 236809 (2007).**
[18] A. Rycerz, J. Tworzydlo, and C. W. J. Beenakker, Nature Physics **3**, 172 (2007).
[19] J. L. Garcia-Pomar, A. Cortijo, and M. Nieto-Vesperinas, Phys. Rev. Lett. **100**, 236801 (2008); Y. S. Ang, S. A. Yang, C. Zhang, Z. Ma, and L. K. Ang, Phys. Rev. B. **96**, 245410 (2017).
[20] Z.-P, Niu, Jour. Appl. Phys. **111**, 103712 (2012); S. P. Milovanovic and F. M. Peeters, Appl. Phys. Lett. **109**, 203108 (2016); M. Settnes, S. R. Power, M. Brandbyge, and A.-P. Jauho, Phys. Rev. Lett. **117**, 276801 (2016); T. Stegmann and N. Szpak, 2D Materials **6**, 015024 (2019).
[21] D. Gunlycke and C. T. White, Phys. Rev. Lett. **106**, 136806 (2011); L. H. Ingaramo and L. E. F. Foa Torres, J. Phys. Condens. Matter **28**, 485302 (2016).
[22] M. M. Grujic, M. Z. Tadic, and F. M. Peeters, Phys. Rev. Lett. **113**, 046601 (2014).
[23] D. Moldovan, M. Ramezani Masir, L. Covaci, and F. M. Peeters, Phys. Rev. B **86**, 115431 (2012); F. Zhai, Y. Ma, and Y.-T. Zhang, JPCM **23**, 385302 (2011); F. Zhai, Nanoscale **4**, 6527 (2012); F. Zhai and K. Chang, Phys. Rev. B **85**, 155415 (2012); Y. Wang, J. App. Phys. **114**, 073709 (2013); W.-T. Lu, Phys. Rev. B **94**, 085403 (2016); M. Settnes, J. H. Garcia, and S. Roche, 2D Materials **4**, 031006 (2017); J. Wang, M. Long, W.-S. Zhao, G. Wang, and K. S. Chan, J. Phys. Condens. Matter **28**, 285302(2016); Q.-P. Wu, Z.-F. Liu, A.-X. Chen, X.-B. Xiao, and Z.-M. Liu, Scientific Reports **6**, 21950 (2016); M. M. Asmar and S. E. Ulloa, Phys. Rev. B **96**, 201407(R) (2017); A. R. S. Lins and J. R. F. Lima, Carbon **160**, 353 (2020); Q.-P. Wu, L.-L. Chang, Y.-Z. Li, X.-B. Xiao, Z.-F. Liu, Physica E **118**, 113864 (2020).
[24] L. Pratley and U. Zulicke, App. Phys. Lett. **104**, 082401 (2014).
[25] Y. Jiang, T. Low, K. Chang, M. I. Katsnelson, and F. Guinea, Phys. Rev. Lett. **110** (2013).
[26] F. Qi and G. Jin, J. App. Phys. **115**, 173701 (2014).
[27] A. Kundu, , H.A. Fertig, and B. Seradjeh, Phys. Rev. Lett. **116** 016802 (2016).
[28] D. Xiao, W. Yao, and Q. Niu, Phys. Rev. Lett. **99, 236809 (2007)**; K. F. Mak, K. L. McGill, J. Park, P.L McEuen, Science **344**, 6191 (2014); Y. Shimazaki, M. Yamamoto, I. V. Borzenets, K. Watanabe, T. Taniguchi, S. Tarucha, Nature Phys **11**, 1032–1036 (2015); Sui, M., Chen, G., Ma, L., Shan, W.-Y., Tian, D., Watanabe, K., Taniguchi, T., Jin, X., Yao, W., Xiao, D., Zhang, Y., Nature Phys **11**, 1027–1031 (2015).
[29] G. Murthy, H. A. Fertig, and E. Shimshoni, Phys. Rev. Research **2**, 013367(2020).
[30] R. Bistritzer and A. H. MacDonald, Proc. Nat. Acad. Sci. USA **108**, 12233 (2011).
[31] P. San-Jose, J. Gonzalez, and F. Guinea, Phys. Rev. Lett.**108**, 216802 (2012).
[32] See Supplementary Material for *Weyl Semimetal Path to Valley Filtering in Graphene* which includes Refs. [33-36]
[33] G. D. Mahan, *Many Particle Physics, Third Edition (Plenum, New York, 2000).*
[34] Hsu, C., Zhen, B., Stone, A. et al. Nat Rev Mater 1, 16048 (2016).
[35] J. R. Schrieffer and P. A. Wolff, Phys. Rev. **149**, 491 (1966).
[36] Tworzydło, J., Trauzettel, B., Titov, M., Rycerz, A. and Beenakker, C., Phys. Rev. Lett. **96** (2006).
[37] For a review, see, S. Manzeli, D. Ovchinnikov, D. Pasquier, O. V. Yazyev, and A. Kis, Nat. Rev. Mater. **2**, 17033 (2017).
[38] Y. Cao, V. Fatemi, S. Fang, K. Watanabe, T. Taniguchi, E. Kaxiras, R. C. Ashoori, and P. Jarillo-Herrero, Nature **556**, 43 (2018); Y. Cao, V. Fatemi, S. Fang, S. L. Tomarken, J. Y. Luo, J. D. Sanchez-Yamagishi, K. Watanabe, T. Taniguchi, E. Kaxiras, R. C. Ashoori, and P. Jarillo-Herrero, Nature **556**, 80 (2018).